JACS
JOURNAL OF THE AMERICAN CHEMICAL SOCIETY
pubs.acs.org/JACS
Article

Two-Dimensional Cobalt(II) Benzoquinone Frameworks for Putative Kitaev Quantum Spin Liquid Candidates

Songwei Zhang, Xu Yang, Brandi L. Wooten, Rabindranath Bag, Lalit Yadav, Curtis E Moore, Smrutimedha Parida, Nandini Trivedi,* Yuanming Lu,* Joseph P. Heremans,* Sara Haravifard,* and Yiying Wu*

Cite This: J. Am. Chem. Soc. 2024, 146, 15061−15069

ABSTRACT: The realization and discovery of quantum spin liquid (QSL) candidate materials are crucial for exploring exotic quantum phenomena and applications associated with QSLs. Most existing metal−organic two-dimensional (2D) quantum spin liquid candidates have structures with spins arranged on the triangular or kagome lattices, whereas honeycomb-structured metal−organic compounds with QSL characteristics are rare. Here, we report the use of 2,5-dihydroxy-1,4-benzoquinone (X_2dhbq, X = Cl, Br, H) as the linkers to construct cobalt(II) honeycomb lattices $(NEt_4)_2[Co_2(X_2dhbq)_3]$ as promising Kitaev-type QSL candidate materials. The high-spin d^7 Co^{2+} has pseudospin-1/2 ground-state doublets, and benzoquinone-based linkers not only provide two separate superexchange pathways that create bond-dependent frustrated interactions but also allow for chemical tunability to mediate magnetic coupling. Our magnetization data show antiferromagnetic interactions between neighboring metal centers with Weiss constants from −5.1 to −8.5 K depending on the X functional group in X_2dhbq linkers (X = Cl, Br, H). No magnetic transition or spin freezing could be observed down to 2 K. Low-temperature susceptibility (down to 0.3 K) and specific heat (down to 0.055 K) of $(NEt_4)_2[Co_2(H_2dhbq)_3]$ were further analyzed. Heat capacity measurements confirmed no long-range order down to 0.055 K, evidenced by the broad peak instead of the λ-like anomaly. Our results indicate that these 2D cobalt benzoquinone frameworks are promising Kitaev QSL candidates with chemical tunability through ligands that can vary the magnetic coupling and frustration.

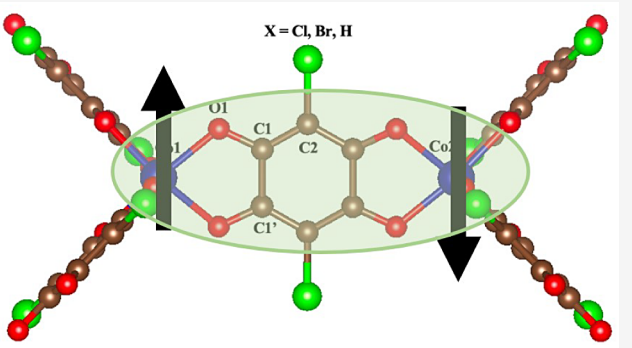

INTRODUCTION

Unlike conventional magnetic materials that usually undergo a phase transition from a magnetically disordered state to a magnetically ordered state at low temperatures, a quantum spin liquid (QSL) is an exotic state of matter where highly entangled electron spins do not develop any long-range magnetic order even in the zero-temperature limit.[1,2] The search for QSL candidates has attracted intensive interest due to their potential for quantum computation applications and also due to their close relation to the microscopic origin of high-temperature superconductivity.[3−5] A few materials exhibiting QSL behaviors have been discovered but mostly with triangular or Kagome structures where neighboring antiferromagnetic interactions cannot be satisfied simultaneously due to the lattice geometry.[2,6−17] In fact, geometric frustration on a nonbipartite lattice with triangular plaquette is the only factor that can result in a QSL phase.[18] As a theoretical breakthrough, Alexei Kiteav showed in a exactly solvable model that a spin-1/2 system on a bipartite honeycomb lattice with bond-dependent Ising interactions can host a QSL ground state.[5] This breakthrough generated considerable activity to design and discover candidate materials for Kitaev QSLs. Among them, iridium oxides[19−22] and α-$RuCl_3$[23−30] with honeycomb structures have turned out to be a promising playground for Kitaev QSLs. Although these materials have been actively discussed as realization of Kitaev QSLs and shown to exhibit promising signatures of QSL states, they nevertheless undergo magnetic ordering at low temperatures in zero external magnetic field, therefore failing to achieve an ideal QSL ground state. This is because there are other non-Kitaev exchange interactions that play a role at low temperatures, such as the antiferromagnetic Heisenberg interaction arising from the direct exchange interaction between the neighboring metal ions, which results in an ordered phase instead of the desired Kitaev QSL state. This

Received: December 24, 2023
Revised: May 13, 2024
Accepted: May 14, 2024
Published: May 24, 2024

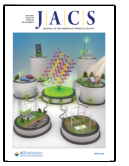

https://doi.org/10.1021/jacs.3c14537
J. Am. Chem. Soc. 2024, 146, 15061−15069

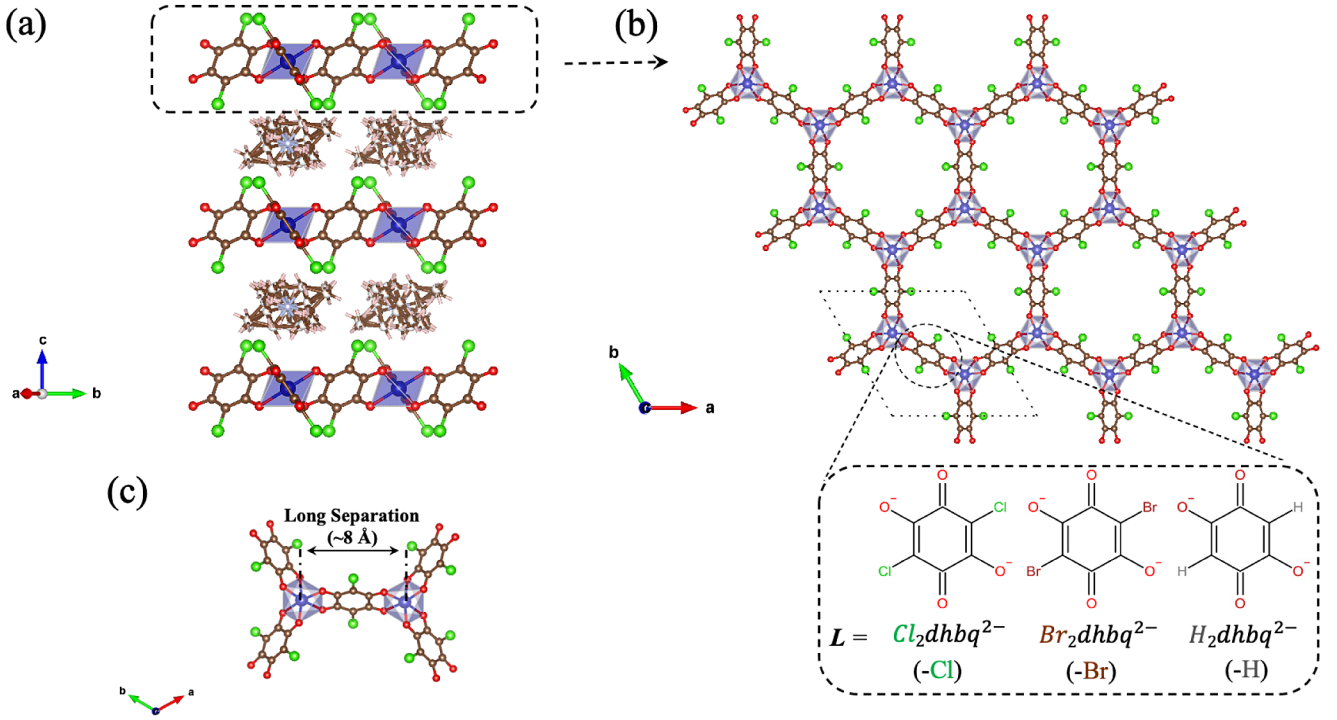

Figure 1. Crystal structures of $(NEt_4)_2[Co_2(Cl_2dhbq)_3]$, as viewed along the crystallographic *ab* plane (a) and *c* axis (b). The blue, green, red, and brown spheres represent Co, Cl, O, and C atoms, respectively. The rounded rectangle in (b) shows the three organic linkers used in compounds **1**, **2**, and **3**, respectively. (c) The local coordination mode of compound **1**. The lengthy separations between Co^{2+} ions reduce the direct overlap between the *d* orbitals of the neighboring metal ions. As a result, the direct exchange interactions are strongly suppressed in MOF structures, opening the possibility of pure Kitaev-type interactions.

motivated us to continue the search for more ideal realizations of the Kitaev model in real materials that may exhibit true spin liquid ground states.

Yamada et al. proposed that two-dimensional metal organic frameworks (MOFs) are an attractive platform for the targeted design of Kitaev QSLs.[31] In contrast to traditional solid-state materials where the Heisenberg interactions compete with Kitaev interactions due to the small size of anions, the electron density of nonmagnetic bridging organic ligands in MOFs can shield the electron cloud tails of the metal ions, thereby substantially reducing the direct overlap between *d* orbitals of the neighboring metal ions. As a result, the direct exchange interaction is strongly suppressed in MOF structures, opening up the possibility of pure Kitaev-type interactions in this material, and positioning the MOFs as the design platform for the realization of Kitaev QSLs with an edge over other inorganic candidates. In addition, MOFs possess a high degree of tunability as they can be built from molecular building blocks. This not only makes it possible to design a structure that can satisfy the basic requirements for Kitaev QSL model but also enables us to fine-tune the magnetic properties. This is another attractive feature of 2D MOFs over inorganic minerals.

Until recently, only a few MOFs have been demonstrated to be QSL candidates and most of them are based on the geometrical frustration from triangular or Kagome lattices.[17,32−38] Shores et al. synthesized Cu(1,3-bdc), the first structurally perfect metal−organic hybrid Kagome with a spin of $S = 1/2$ on lattice vertices, demonstrating spin-frustrated behavior with ferromagnetic ordering transition at low temperatures.[17] Misumi et al. identified 2D honeycomb $Cu_3(HHTP)_2$ with a Kagome lattice as a QSL candidate performing magnetic susceptibility and specific heat measurements.[36] Sorolla et al. reported on a half-spin Kagome lattice, $[(CH_3)_2(NH_2)]_3[Cu^{II}_3(\mu_3{-}OH)(\mu_3\text{-}SO_4)(\mu_3\text{-}SO_4)_3]\cdot 0.24H_2O$, showing antiferromagnetic interactions but no magnetic ordering or spin freezing down to 2K, indicating it as a promising QSL candidate.[37] Zhang et al. found no long-range ordering in the copper-oxalate framework, $[(C_2H_5)_3NH]_2Cu_2(C_2O_4)_3$ down to 2K, with a frustration factor greater than 3000, highlighting its potential of varying MOF's dimensionality to obtain QSL.[34] Burzuri et al. identified [PNP][CoRh(ox)$_3$], a 2D heterometallic oxalate framework as an appealing QSL system by a combination of electronic paramagnetic resonance, specific heat and AC magnetic susceptibility measurements in a wide range of frequencies and temperatures.[38]

This work reports the use of 2,5-dihydroxy-1,4-benzoquinone (X_2dhbq, X = Cl, Br, H) as the linkers to construct cobalt(II) honeycomb lattices (compounds **1**−**3**, respectively, see Figure 1a−c). These linkers not only provide separate pathways for superexchange interactions between metal centers but also provide chemical tunability by varying the functional group X in X_2dhbq at the 3 and 6 positions (Figure 1b). Different electron-withdrawing groups can be used to tune the energetics of the linkers' frontier orbitals. Their bis-bidentate coordination around high spin d^7 Co^{2+} in an octahedral crystal field results in a $(t_{2g})^5$ $(e_g)^2$ configuration with $S = 3/2$ and an effective $L = 1$ moments, forming pseudo spin-1/2 doublets in their ground state.[39] Therefore, these two-dimensional (2D) cobalt benzoquinone MOFs are promising Kitaev-type QSL candidate materials. $(NEt_4)_2[Co_2(X_2dhbq)_3]$ (X = Cl, Br, H) was successfully synthesized via a solution method. Single-crystal X-ray diffraction studies revealed that each Co^{2+} center is octahedrally coordinated with two oxygen donors from each

https://doi.org/10.1021/jacs.3c14537
J. Am. Chem. Soc. 2024, 146, 15061−15069

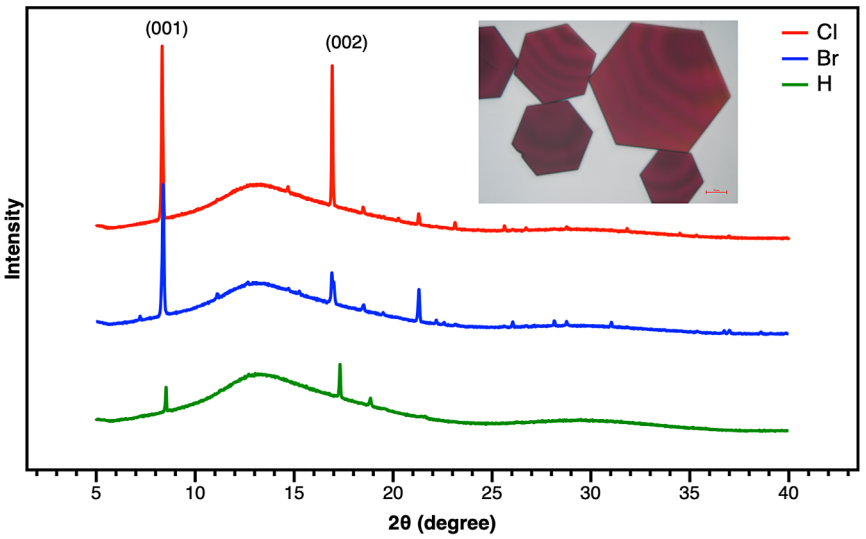

Figure 2. Powder X-ray diffraction data for **1** (−Cl), **2** (−Br), and **3** (−H). All samples show preferred orientation due to the flat shape of MOF particles (inset: the image of compound **1** crystals; the scale bar is 10 μm).

Table 1. Selected Interatomic Distances (Å) and Vibrational Frequencies (cm^{-1}) for Compounds 1−3[a]

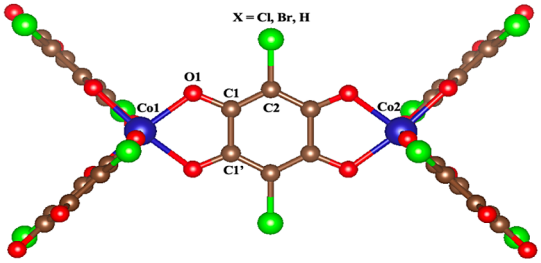

	1 (-Cl)	2 (-Br)	3 (-H)
Co1-O1	2.061(7)	2.063(7)	2.069(15)
C1-O1	1.264(12)	1.234(9)	1.34(4)
C1-C2	1.381(14)	1.390(14)	1.32(3)
C1-C1'	1.520(10)	1.567(12)	1.54(5)
Co1-Co2	7.8837(12)	7.8708(3)	7.911(7)
$\nu_{(C-O)}$	1605	1601	1579
$\nu_{(C-C)}$	1357	1335	1394

[a]The labels of the atoms are shown on the left side

of three X_2dhbq^{2-} linkers, and this coordination mode gives rise to 2D honeycomb-like layers, thereby creating the building blocks for the Kitaev QSL model. Direct current (DC) magnetic susceptibility experiments reveal no long-range magnetic ordering down to 300 mK even when the nearest neighbor's antiferromagnetic interactions are strong. In addition, zero field cooled/field cooled (ZFC/FC) DC magnetization measurements indicate no spin glass transition. Heat capacity measurements further confirmed that this is a half spin system with no long-range order for $(NEt_4)_2[Co_2(H_2dhbq)_3]$ down to 0.055 K.

EXPERIMENTAL SECTION

Synthetic Procedure. To a 23 mL glass vial, a solid (137 mg, 0.845 mmol) of $(EtN_4)Cl$ was dissolved in 16 mL *N,N*-dimethylformamide (DMF), followed by the successive addition of a DMF solution (0.5 mL) of $Co(NO_3)_2$ $6H_2O$ (26 mg, 0.0893 mmol), a DMF solution (1.0 mL) of chloranilic acid (28 mg, 0.134 mmol), and 0.8 mL deionized water. The resulting solution was shaken and then placed in an oven at 130 °C for 24 h. After the reaction mixture was allowed to cool to ambient temperature, the mother liquor was decanted and then replenished with fresh DMF. This decanting−replenishing procedure was repeated until the supernatant was colorless to afford compound **1**, $(NEt_4)_2[Co_2(Cl_2dhbq)_3]$, as brown hexagonal plate-shaped crystals suitable for single-crystal X-ray diffraction. Compound **2**, $(NEt_4)_2[Co_2(Br_2dhbq)_3]$ was synthesized as brown hexagonal plate-shaped crystals according to the described procedure for **1** using $Co(NO_3)_2$ $6H_2O$, bromanilic acid, and $(EtN_4)Br$. Compound **3**, $(NEt_4)_2[Co_2(H_2dhbq)_3]$ was synthesized as brown hexagonal plate-shaped crystals according to the described procedure for **1** using $Co(NO_3)_2$ $6H_2O$, anilic acid, and $(EtN_4)Cl$.

Characterization Methods. Raman spectra were recorded using a Renishaw inVia microscope with an incident wavelength of 633 nm. XRD measurements were performed on a Bruker D8 ADVANCE powder diffractometer (40 kV, 40 mA, sealed Cu X-ray tube) equipped with a LYNXEYE XET position sensitive detector. Data were collected with an incident beam monochromator (Johansson type SiO2-crystal). The single crystal X-ray diffraction studies were carried out on a Bruker Kappa Photon III CPAD diffractometer equipped with Mo K_α radiation (λ = 0.71073 Å).

Physical and Magnetic Property Measurements. Magnetic measurements in the temperature range of 3−300 K were carried out on a polycrystalline sample powder sealed in a gelatin capsule. The data were collected by using a Quantum Design MPMS3 superconducting quantum interference device (SQUID) magnetometer. Zero-field-cooled and field-cooled measurements were carried out with an applied field of 1000 Oe. Low-temperature magnetic measurements were carried out on polycrystalline sample using Helium-3 (^{3}He) option attached to SQUID magnetometer in the temperature range 300 mK to 2 K.

Specific heat measurements above 2 K were conducted on a Quantum Design Physical Properties Measurement System (PPMS) with a calibrated HC puck. The sample was pressed into a pellet and then broken apart to select the appropriate size for the instrument. Special care was taken to calibrate both the puck and the puck plus wax in the field before adding the sample. Below 2 K, the heat capacity data from 55 mK to 4 K were collected using dilution refrigerator (DR) option attached to PPMS Dynacool system. To

https://doi.org/10.1021/jacs.3c14537
J. Am. Chem. Soc. 2024, 146, 15061−15069

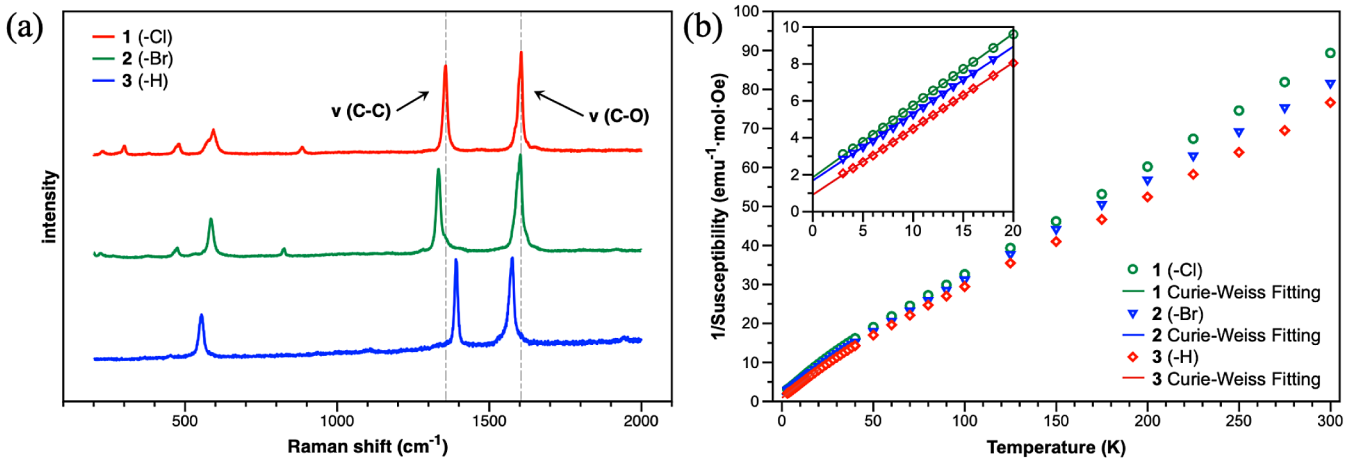

Figure 3. (a) Raman spectra for compounds **1** (−Cl, red), **2** (−Br, green), and **3** (-H, blue). (b) Variable-temperature (3−300 K) inverse molar magnetic susceptibility for compounds **1**−**3.** (The inset shows a zoom-in view of the low temperature region below 20 K with the lines from the Curie−Weiss fitting of low temperature data for each compound.)

obtain strong sample coupling between the sample and heat capacity platform, low temperature "N" grease is used.

RESULTS AND DISCUSSION

Synthesis and Crystal Structure. The reaction of cobalt(II) nitrate and different benzoquinone derivatives (X_2dhbq^{2-}: X = Cl, Br, H) in DMF in a glass vial at 130 °C produced red-brown hexagonal plate-type crystals of compound **1** $(NEt_4)_2[Co_2(Cl_2dhbq)_3]$, **2** $(NEt_4)_2[Co_2(Br_2dhbq)_3]$, and **3** $(NEt_4)_2[Co_2(H_2dhbq)_3]$ with an *ab* dimension of around 50 μm (Figure 2, inset). Compounds **1**−**3**, $(NEt_4)_2[Co_2(X_2dhbq)_3]$ (X = Cl, Br, H) are isostructural and crystallized in the trigonal space group $P\bar{3}1m$, composed of anionic honeycomb-like layers and quaternary ammonium counter cations (Figure 1a,b). Within anionic layers, each Co atom is coordinated with three bridging ligands through the O atoms to form an octahedral geometry. These layers are extended along the crystallographic *ab* plane and stacked along the crystallographic *c* axis in an eclipsed AA stacking mode. As a countercation, each tetraethylammonium (Et_4N^+) situated at the center of two nearest Co atoms from adjacent layers, giving an interlayer spacing of 10.18 Å. Selected interatomic distances are given in Table 1. All compounds show similar Co−O distances, indicating similar orbital overlaps between the Co centers and their surrounding ligands. Notably, a similar structure as found for compound **1** has been reported previously through a postsynthetic metal-exchange approach.[40] Powder X-ray diffraction (Figure 2) confirmed the purity of the bulk materials, and the presence of Bragg peaks (00*l*) indicated a preferential crystallographic orientation of crystals, in agreement with the feature of the 2D structure.

Raman Spectroscopy. Considering that benzoquinone ligands are redox active, solid-state Raman spectra (Figure 3a) were collected for each compound to confirm the oxidation states of ligands for compounds **1**−**3**. The Raman bands associated with the C−C and C−O vibrations have been widely used to assign the oxidation states of benzoquinone ligands. The bands centered at 1330−1400 and 1550−1620 cm^{-1} are attributed to the C−C and C−O stretching modes, respectively. Based on the assignments of Raman bands for the isostructural benzoquinoid frameworks,[41−44] the ligands are doubtlessly confirmed to be in the X_2dhbq^{2-} state for all the compounds. It is noteworthy that though the C−C and C−O bands situate within the same range for compounds **1**−**3**, the shifts of band positions are clearly observable in the spectra (Table 1). The C−C and C−O bands of compound **1** locate at 1357 and 1605 cm^{-1}, respectively. Compared to the band positions of compound **1**, the C−C band shifts to lower wavenumbers, 1335 cm^{-1} and the C−O band remains unchanged for compound **2**, while the C−C and C−O bands of compound **3** shift to higher wavenumbers (Table 1), 1394 cm^{-1} and lower wavenumbers, 1579 cm^{-1}, respectively. Correspondingly, as the crystallographic data show, the C−C bond shortens from 1.38 Å in compound **1** to 1.32 Å in compound **3** while the C−O bond elongates from 1.26 Å in compound **1** to 1.34 Å in compound **3**. This indicated that changing the substituents on the ligands remarkably affects its electron delocalization.

Magnetic Properties. To investigate the evidence of cobalt(II) benzoquinone compounds as QSL candidates, DC magnetization measurements were performed for the powder sample over different temperature ranges. Figure 3b shows the inverse of temperature-variable magnetic susceptibility $\chi_{(T)}$ data for compounds **1**−**3** between 2 and 300 K. No magnetic transition temperatures can be observed down to 3 K, indicating the absence of long-range magnetic ordering for all the compounds. Also, the zero-field-cooled curves overlap with the field-cooled curves, indicating that there is no spin freezing for all the compounds, thereby indicating that disorder is not playing a dominant role. Curie−Weiss law is used to fit the $1/\chi_{(T)}$−T plots in the temperature range of above 100 K (high-temperature range, HT) and around 10 K (low-temperature range, LT) because the slope change is observed at around 50 K for all the compounds. The effective magnetic moment (μ_{eff}) and Weiss constant (θ_{CW}) are obtained from the fitting (see the next two sections) and summarized in Tables 2 **and** 3. The negative values of the Weiss constant indicate dominant antiferromagnetic interactions between neighboring metal centers. The change of the slope indicates different μ_{eff} values in different temperature ranges, which is due to the crossover from the S = 3/2, L = 1 state in each Co^{2+} ion described in the HT range to a Kramers-doublet state with an effective spin-1/2 per Co^{2+} ion in the LT range. The occurrence of two non-long-range order regimes has been observed in many quantum magnets with strong spin−orbit

https://doi.org/10.1021/jacs.3c14537
J. Am. Chem. Soc. 2024, 146, 15061−15069

Table 2. Effective Magnetic Moment, μ_{eff} (μ_B) and Curie-Weiss Constant, θ_{CW} (K) Obtained from the Fit at the Temperature Range 15−40 K for Compounds 1−3

ligands	θ_{CW} (K)	3J+K (meV)	μ_{eff} /μ_B
1 (−Cl)	−8.5	2.91	4.88
2 (−Br)	−7.6	2.63	4.97
3 (−H)	−5.1	1.75	5.00

Table 3. Trigonal Field Distortion Δ, the Spin-Orbital Coupling λ, and the Constant Part χ_0 Obtained from the Susceptibility Fit at the Temperature Range 15−300 K for Compounds 1−3

ligands	χ_0 (emu/mol·Oe)	λ (meV)	Δ (meV)
1 (−Cl)	1.9×10^{-3}	12.5	15.5
2 (−Br)	3.2×10^{-3}	10.6	17.8
3 (−H)	4.6×10^{-3}	8.5	10.9

coupling (SOC) effect.[45−47] Also, the difference in μ_{eff} and θ_{CW} from compounds **1** to **3** indicated that different functional groups of the ligands modulate the energy matching between the ligands and magnetic centers through the superexchange pathways, finally tuning the hopping energies and magnetic frustration.

Symmetry Analysis. The space group of our compounds is the symmorphic group $P\bar{3}1m$, whose corresponding point group symmetry is D_{3d}. Due to spin−orbital coupling and spatial anisotropy, we have bond-dependent exchange interactions closely resembling the Kitaev model. We set up the coordinate system as in Figure 4. The Z-bond has two

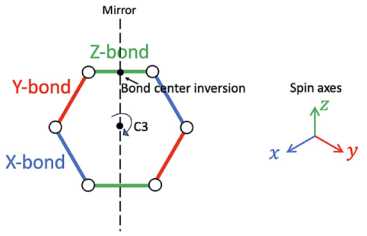

Figure 4. $S = 1/2$ pseudospins on a honeycomb lattice with nearest-neighbor bond-dependent exchange interactions. We have used a cubic coordinate system for pseudospins, where each pseudospin axes are perpendicular to the corresponding bonds. The Z-bond is invariant under two symmetries: a mirror plane and a bond-center inversion. The X- and Y-bonds are related to the Z-bond by C3 rotation symmetries.

symmetries: a mirror plane that is perpendicular to the bond and a bond-center inversion. The mirror symmetry exchanges two sites and changes spin directions in the following way: (S^x, S^y, S^z) → ($-S^y$,$-S^x$, $-S^z$). And the inversion symmetry exchanges two sites. The exchange interactions for a Z-bond respecting symmetries is therefore

$$H_{ij}^{z} = J\vec{S}_i \cdot \vec{S}_j + KS_i^z S_j^z + \Gamma(S_i^x S_j^y + S_j^x S_i^y) + \Gamma' (S_i^x S_j^z + S_j^x S_i^z + S_i^y S_j^z + S_j^y S_i^z)$$

Here, J denotes the Heisenberg interaction, K denotes the Kitaev interaction, and Γ, Γ' denote two different types of symmetric off-diagonal exchange interactions.

Exchange interactions for X- and Y-bonds are obtained from cyclic permutation among S^x, S^y, S^z, as is obvious from the C3 symmetry.

Magnetic Susceptibility Fitting. The low temperature physics can be captured well by the exchange model of pseudospin-1/2. We use the Curie−Weiss law $\chi = \frac{\mu_{eff}^2}{3k_B(T-\Theta_{CW})}$ to fit the data between temperature range 15−40 K, where the data show a very good linear behavior (Figure 3b inset). For the data taken from a powdered sample, we average the magnetic susceptibility tensor χ over all directions and extract μ_{eff} and the averaged exchange interactions 3J+K from the fitting. Note that in the high temperature expansion, the averaged susceptibility in the powder sample does not depend on the exchange parameters Γ and Γ′. The fitting results are given in Table 2. It is notable that when the functional group of the linker is varied from −Cl to −Br and to −H with decreasing electronegativity, there is a systematic decrease in exchange interactions with the Curie−Weiss constant changing from −8.5 to −7.6 and to −5.1 K. For comparison, the low-temperature physics of inorganic Co^{2+} honeycomb materials such as $Na_2Co_2TeO_6$ can be similarly described by an effective spin-1/2 model on a honeycomb lattice. However, in case of $Na_2Co_2TeO_6$, the Co^{2+} ions develop long-range magnetic ordering at low temperatures, contrary to the Co-based MOF systems reported here.[48] Although bond-dependent Kitaev interactions are naturally present in $Na_2Co_2TeO_6$, additional exchange interactions apart from Kitaev interactions give rise to the magnetic long-range orders.[49] Therefore, the absence of magnetic ordering at low temperatures in our Co-based MOF compounds indicates that MOFs can be considered as more promising candidates for the realization of Kitaev physics.

To account for susceptibility at temperatures up to 300 K, it is necessary to take atomic physics into consideration. Therefore, we start from the $(t_{2g})^5$ $(e_g)^2$ configurations with $S = 3/2$ and $L = 1$ and take into consideration the trigonal field distortion $H_\Delta = \Delta\left(L_z^2 - \frac{2}{3}\right)$ and spin−orbital coupling $H_\lambda = \lambda\vec{L}\cdot\vec{S}$.[50] We then solve this Hamiltonian and fit the data within the temperature range 15−300 K using the method of least squares. In our fitting, we have also included a temperature-independent constant χ_0 to account for ionic physics with higher energy scales. The negative sign of Δ is because trigonal field distortion can be viewed by a slight compression of the O_6 octahedron along the crystalline c-axis, as can be seen in Table 1. And the results are listed in Table 3.

Low-T Susceptibility and Specific Heat of Compound 3. The low-temperature magnetization measurements were performed on compound **3** in the temperature range of 0.3−2 K, as shown in Figure 5a. No divergence and inconsistency can be observed down to 0.3 K for the ZFC and FC curves, indicating the absence of any long-range magnetic ordering down to 0.3 K. Specific heat measurements are a useful probe for observing magnetic transitions in the search for quantum spin liquids.[1] Figure 5b shows the temperature dependence of specific heat $C_p(T)$ in the presence of various magnetic fields of 0, 1, 2, 3, 5, and 9 T from 0.055 to 4 K for compound **3**. The $C_p(T)$ data taken at 9T decrease monotonically with decreasing temperature following a T^3 law and are thus attributed to the phonon contribution, which is seen to be negligible below 2K. It is noteworthy to add that in Figure 5B, the data were extended to higher temperatures but were cut off to emphasize the spin contributions. The $C_p(T)$ flattens at low

https://doi.org/10.1021/jacs.3c14537
J. Am. Chem. Soc. 2024, 146, 15061−15069

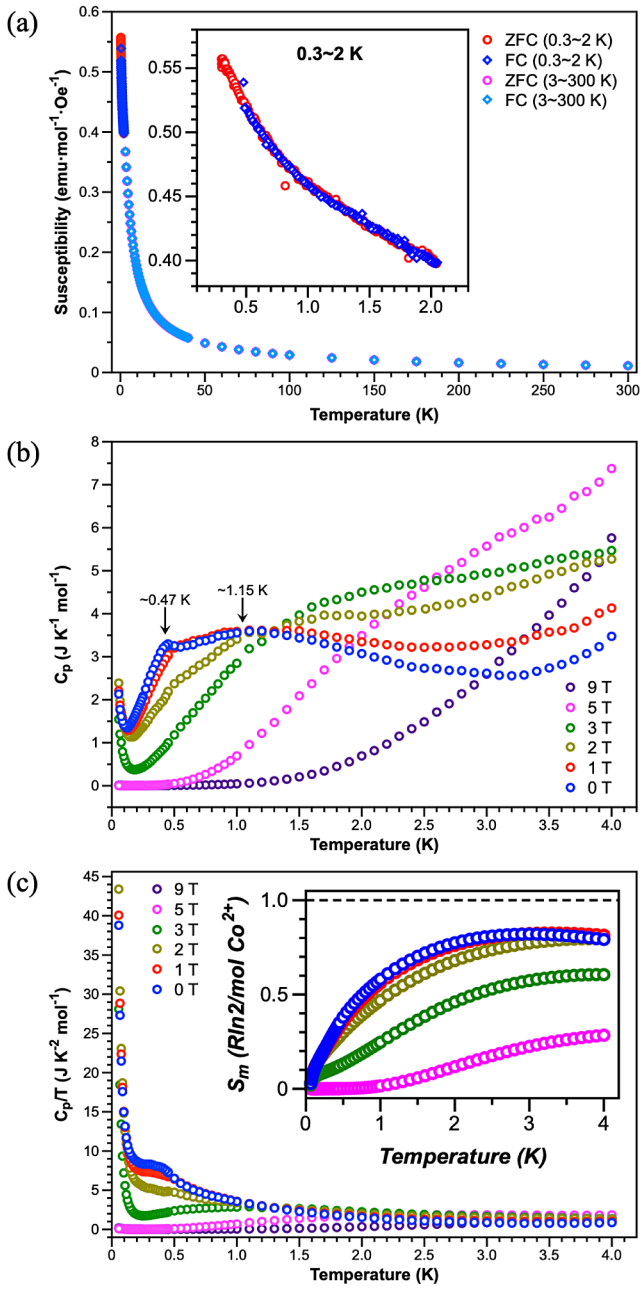

Figure 5. (a) Low-temperature (0.3−2 K) zero-field-cooled/field-cooled (ZFC/FC) molar magnetic susceptibility for compound **3**. The expanded view of long temperature (0.3−2 K) data is shown in the inset. (b) C_p versus T plot at low temperature (0.055−4 K) at various magnetic fields (0, 1, 2, 3, 5, 9 T) for compound **3**. (c) C_p/T versus T and S_m versus T plots at low temperature (0.055−4 K) at various magnetic fields (0, 1, 2, 3, 5, 9 T) for compound **3**. The calculated entropy is shown in the inset, as collected for various applied magnetic fields.

temperatures (below 0.5 K) and high fields (5 and 9 T), as expected. However, an upturn in $C_p(T)$ is observed at low temperatures (below 0.1 K) and low fields (below 3 T). This upturn tail might be a manifestation of a frustrated magnetic lattice.[51] No sharp λ-like anomaly is observed down to 0.055 K from the $C_p(T)$ data, indicating the absence of long-range magnetic ordering. Instead, a broad hump appears at around 1.15 K and shifts to higher temperatures with increasing the magnetic field, which could be attributed to the short-range correlations or the onset of quantum fluctuation in QSL systems.[52] The occurrence of a hump in $C_p(T)$ plot might be a characteristic feature of a spin-frustrated system, which has been noticed in some QSL systems.[52−56] Furthermore, a small kink is observed at ∼0.47 K, just before the hump maximum at ∼1.15 K, which might be associated with an unusual thermodynamic phase transition different from the long-range order, with significant short-range correlations.[53] To clarify the low temperature regions and upturn, C_p/T vs T plot is shown separately in Figure 5c and the calculated entropy (the integral of C_p/T dT) is shown in the inset with various fields. The entropy calculated at a high magnetic field (9T) was used to represent the phonon contribution. The spin entropy is then obtained by subtracting this value from the total entropy at 0, 1, 2, 3, and 5 T. The spin entropy decreased with increasing magnetic field. The calculated entropy seems to be saturated near Rln2 agreeing with the $S = 1/2$ state of Co^{2+} magnetic ions. However, a further quantitative analysis is hindered because we were unable to accurately extract the magnetic contribution for the specific heat due to the absence of a suitable nonmagnetic analog of the compounds. Therefore, more measurements on an MOF with similar structure but no magnetic additions will be needed to subtract the phonon contribution from the total specific heat and have a better understanding of the overall trends.

Sub-2K magnetization measurements for compounds **1** and **2** have also been carried out (Figure S1). The DC-susceptibility results show no signature of long-range magnetic ordering down to lowest temperature accessible (300 mK). The frustration factor ($f = |\theta_{CW}|/T_N$ with T_N = lowest temperature measured) reaches 28, 25, and 17 for compounds **1**, **2**, and **3**, respectively, demonstrating that these MOFs are highly frustrated. The specific heat experiments for all samples were also been completed. As shown in Figure S2, all three MOFs show similar behavior.

CONCLUSION

In summary, the magnetic and specific heat properties were investigated, for the first time, on a series of 2D honeycomb cobalt benzoquinone MOFs, $(NEt_4)_2[Co_2(X_2dhbq)_3]$ (X = Cl, Br, H) with effective spin-1/2. Magnetization experiments showed the antiferromagnetic interactions between neighboring metal centers, but no magnetic transitions and spin freezing could be observed down to 0.3 K. Heat capacity measurements further confirmed that there's no long-range order for $(NEt_4)_2[Co_2(H_2dhbq)_3]$ down to 0.055 K, evidenced by the broad peak instead of λ-like anomaly. These results indicate that the cobalt benzoquinone MOFs might be promising as QSL candidates. However, it should be noted that the true ground state remains to be confirmed and that short-range magnetic ordering or spin freezing cannot be conclusively ruled out based on the present data. Moreover, the potential presence of stacking faults or other possible disorders could lead to random exchange between the cobalt pseudospins, potentially resulting in the formation of a spin-liquid-like state (e.g., random-singlet state), distinct from the Kitaev QSL. To get more insights into the spin structures and excitations, we will explore this system extensively in the future. Therefore, larger crystals need to be grown, and further experiments at different energy scales and along different orientations, such as inelastic neutron scattering, will be performed.

https://doi.org/10.1021/jacs.3c14537
J. Am. Chem. Soc. 2024, 146, 15061−15069

■ ASSOCIATED CONTENT

Supporting Information

The Supporting Information is available free of charge at https://pubs.acs.org/doi/10.1021/jacs.3c14537.

Experimental summary of single crystal X-ray diffraction studies; Tables S1−S15; thermodynamic measurements of compounds **1** and **2**; Figures S1 and S2 (PDF)

Accession Codes

CCDC 2320927−2320929 contain the supplementary crystallographic data for this paper. These data can be obtained free of charge via www.ccdc.cam.ac.uk/data_request/cif, or by emailing data_request@ccdc.cam.ac.uk, or by contacting The Cambridge Crystallographic Data Centre, 12 Union Road, Cambridge CB2 1EZ, UK; fax: +44 1223336033.

■ AUTHOR INFORMATION

Corresponding Authors

Nandini Trivedi − *Department of Chemistry & Biochemistry, The Ohio State University, Columbus, Ohio 43210, United States*; Email: trivedi.15@osu.edu

Yuanming Lu − *Department of Physics, The Ohio State University, Columbus, Ohio 43210, United States*; Email: lu.1435@osu.edu

Joseph P. Heremans − *Department of Mechanical & Aerospace Engineering, The Ohio State University, Columbus, Ohio 43210, United States*; Email: heremans.1@osu.edu

Sara Haravifard − *Department of Physics, Duke University, Durham, North Carolina 27708, United States*; Email: sara.haravifard@duke.edu

Yiying Wu − *Department of Chemistry & Biochemistry, The Ohio State University, Columbus, Ohio 43210, United States*; orcid.org/0000-0001-9359-1863; Email: wu@chemistry.ohio-state.edu

Authors

Songwei Zhang − *Department of Chemistry & Biochemistry, The Ohio State University, Columbus, Ohio 43210, United States*; orcid.org/0000-0001-5930-826X

Xu Yang − *Department of Physics, The Ohio State University, Columbus, Ohio 43210, United States*

Brandi L. Wooten − *Department of Materials Science and Engineering, The Ohio State University, Columbus, Ohio 43210, United States*

Rabindranath Bag − *Department of Physics, Duke University, Durham, North Carolina 27708, United States*

Lalit Yadav − *Department of Physics, Duke University, Durham, North Carolina 27708, United States*

Curtis E Moore − *Department of Chemistry & Biochemistry, The Ohio State University, Columbus, Ohio 43210, United States*; orcid.org/0000-0002-3311-7155

Smrutimedha Parida − *Department of Chemistry & Biochemistry, The Ohio State University, Columbus, Ohio 43210, United States*

Complete contact information is available at: https://pubs.acs.org/10.1021/jacs.3c14537

Notes

The authors declare no competing financial interest.

■ ACKNOWLEDGMENTS

This work was supported by Centre for Emergent Materials at The Ohio State University, a National Science Foundation (NSF) MRSEC through NSF Award No. DMR-2011876.

■ REFERENCES

(1) Chamorro, J. R.; McQueen, T. M.; Tran, T. T. Chemistry of Quantum Spin Liquids. *Chem. Rev. Am. Chem. Soc.* **2021**, *121*, 2898.

(2) Balents, L. Spin Liquids in Frustrated Magnets. *Nature* **2010**, *464*, 199208. .

(3) Anderson, P. W. The Resonating Valence Bond State in La2CuO4 and Superconductivity. *Science* **1987**, *235* (4793), 1196−1198.

(4) Kitaev, A. Y. Fault-Tolerant Quantum Computation by Anyons. *Ann. Phys.* **2003**, *303* (1), 2−30.

(5) Kitaev, A. Anyons in an Exactly Solved Model and Beyond. *Ann. Phys.* **2006**, *321* (1), 2−111.

(6) Janson, O.; Richter, J.; Sindzingre, P.; Rosner, H. Coupled Frustrated Quantum Spin-$\frac{1}{2}$ Chains with Orbital Order in Volborthite ${\text{Cu}}_{3}{\text{V}}_{2}{\text{O}}_{7}-{(\text{OH})}_{2}\ensuremath{\cdot}2{\text{H}}_{2}\text{O}$. *Phys. Rev. B* **2010**, *82* (10), 104434.

(7) Li, Y.; Adroja, D.; Bewley, R. I.; Voneshen, D.; Tsirlin, A. A.; Gegenwart, P.; Zhang, Q. Crystalline Electric-Field Randomness in the Triangular Lattice Spin-Liquid YbMgGaO4. *Phys. Rev. Lett.* **2017**, *118* (10), 1−7.

(8) Nakatsuji, S.; Kuga, K.; Kimura, K.; Satake, R.; Katayama, N.; Nishibori, E.; Sawa, H.; Ishii, R.; Hagiwara, M.; Bridges, F.; et al. Spin-Orbital Short-Range Order on a Honeycomb-Based Lattice. *Science* **2012**, *336* (6081), 559−563.

(9) Isono, T.; Kamo, H.; Ueda, A.; Takahashi, K.; Kimata, M.; Tajima, H.; Tsuchiya, S.; Terashima, T.; Uji, S.; Mori, H. Gapless Quantum Spin Liquid in an Organic Spin-1/2 Triangular-Lattice κ-H3 (Cat-EDT-TTF)2. *Phys. Rev. Lett.* **2014**, *112* (17), 1−5.

(10) Yamashita, M.; Nakata, N.; Senshu, Y.; Nagata, M.; Yamamoto, H. M.; Kato, R.; Shibauchi, T.; Matsuda, Y. Highly Mobile Gapless Excitations in a Two-Dimensional Candidate Quantum Spin Liquid. *Science* **2010**, *328* (5983), 1246−1248.

(11) Itou, T.; Oyamada, A.; Maegawa, S.; Tamura, M.; Kato, R. Quantum Spin Liquid in the Spin-$1/2$ Triangular Antiferromagnet $\mathrm{Et}{\mathrm{Me}}_{3}\mathrm{Sb}{[\mathrm{Pd}-{(\text{dmit})}_{2}]}_{2}$. *Phys. Rev. B* **2008**, *77* (10), 104413.

(12) Shimizu, Y.; Hiramatsu, T.; Maesato, M.; Otsuka, A.; Yamochi, H.; Ono, A.; Itoh, M.; Yoshida, M.; Takigawa, M.; Yoshida, Y.; et al. Pressure-Tuned Exchange Coupling of a Quantum Spin Liquid in the Molecular Triangular Lattice κ- (ET)2Ag2 (CN)3. *Phys. Rev. Lett.* **2016**, *117* (10), 1−6.

(13) Shimizu, Y.; Miyagawa, K.; Kanoda, K.; Maesato, M.; Saito, G. Spin Liquid State in an Organic Mott Insulator with a Triangular Lattice. *Phys. Rev. Lett.* **2003**, *91*, 10.

(14) Yamashita, S.; Nakazawa, Y.; Oguni, M.; Oshima, Y.; Nojiri, H.; Shimizu, Y.; Miyagawa, K.; Kanoda, K. Thermodynamic Properties of a Spin-1/2 Spin-Liquid State in a κ-Type Organic Salt. *Nat. Phys.* **2008**, *4* (6), 459−462.

(15) Pratt, F. L.; Baker, P. J.; Blundell, S. J.; Lancaster, T.; Ohira-Kawamura, S.; Baines, C.; Shimizu, Y.; Kanoda, K.; Watanabe, I.; Saito, G. Magnetic and Non-Magnetic Phases of a Quantum Spin Liquid. *Nature* **2011**, *471* (7340), 612−616.

(16) Han, T. H.; Helton, J. S.; Chu, S.; Nocera, D. G.; Rodriguez-Rivera, J. A.; Broholm, C.; Lee, Y. S. Fractionalized Excitations in the Spin-Liquid State of a Kagome-Lattice Antiferromagnet. *Nature* **2012**, *492* (7429), 406−410.

(17) Shores, M. P.; Nytko, E. A.; Bartlett, B. M.; Nocera, D. G. A Structurally Perfect S = 1/2 Kagomé Antiferromagnet. *J. Am. Chem. Soc.* **2005**, *127* (39), 13462−13463.

(18) Wen, J.; Yu, S.-L.; Li, S.; Yu, W.; Li, J.-X. Experimental Identification of Quantum Spin Liquids. *NPJ. Quantum Mater.* **2019**, *4* (1), 12.

(19) Biffin, A.; Johnson, R. D.; Kimchi, I.; Morris, R.; Bombardi, A.; Analytis, J. G.; Vishwanath, A.; Coldea, R. Noncoplanar and Counterrotating Incommensurate Magnetic Order Stabilized by Kitaev Interactions in γ-Li2iro3. *Phys. Rev. Lett.* **2014**, *113* (19), 1−5.
(20) Hwan Chun, S.; Kim, J. W.; Kim, J.; Zheng, H.; Stoumpos, C. C.; Malliakas, C. D.; Mitchell, J. F.; Mehlawat, K.; Singh, Y.; Choi, Y.; et al. Direct Evidence for Dominant Bond-Directional Interactions in a Honeycomb Lattice Iridate Na 2 IrO 3. *Nat. Phys.* **2015**, *11* (6), 462−466.
(21) Modic, K. A.; Smidt, T. E.; Kimchi, I.; Breznay, N. P.; Biffin, A.; Choi, S.; Johnson, R. D.; Coldea, R.; Watkins-Curry, P.; McCandless, G. T.; et al. Realization of a Three-Dimensional Spin-Anisotropic Harmonic Honeycomb Iridate. *Nat. Commun.* **2014**, *5* (May), 1−6.
(22) Choi, S. K.; Coldea, R.; Kolmogorov, A. N.; Lancaster, T.; Mazin, I. I.; Blundell, S. J.; Radaelli, P. G.; Singh, Y.; Gegenwart, P.; Choi, K. R.; et al. Spin Waves and Revised Crystal Structure of Honeycomb Iridate Na 2IrO 3. *Phys. Rev. Lett.* **2012**, *108* (12), 1−5.
(23) Plumb, K. W.; Clancy, J. P.; Sandilands, L. J.; Shankar, V. V.; Hu, Y. F.; Burch, K. S.; Kee, H. Y.; Kim, Y.-J.-A. RuCl3: A Spin-Orbit Assisted Mott Insulator on a Honeycomb Lattice. *Phys. Rev. B - Condens. Matter Mater. Phys.* **2014**, *90* (4), 1−5.
(24) Johnson, R. D.; Williams, S. C.; Haghighirad, A. A.; Singleton, J.; Zapf, V.; Manuel, P.; Mazin, I. I.; Li, Y.; Jeschke, H. O.; Valentí, R.; et al. Monoclinic Crystal Structure of α-RuCl3 and the Zigzag Antiferromagnetic Ground State. *Phys. Rev. B - Condens. Matter Mater. Phys.* **2015**, *92* (23), 1−12.
(25) Sandilands, L. J.; Tian, Y.; Plumb, K. W.; Kim, Y. J.; Burch, K. S. Scattering Continuum and Possible Fractionalized Excitations in α-RuCl3. *Phys. Rev. Lett.* **2015**, *114* (14), 1−6.
(26) Nasu, J.; Knolle, J.; Kovrizhin, D. L.; Motome, Y.; Moessner, R. Fermionic Response from Fractionalization in an Insulating Two-Dimensional Magnet. *Nat. Phys.* **2016**, *12* (10), 912−915.
(27) Banerjee, A.; Bridges, C. A.; Yan, J. Q.; Aczel, A. A.; Li, L.; Stone, M. B.; Granroth, G. E.; Lumsden, M. D.; Yiu, Y.; Knolle, J.; et al. Proximate Kitaev Quantum Spin Liquid Behaviour in a Honeycomb Magnet. *Nat. Mater.* **2016**, *15* (7), 733−740.
(28) Cao, H. B.; Banerjee, A.; Yan, J. Q.; Bridges, C. A.; Lumsden, M. D.; Mandrus, D. G.; Tennant, D. A.; Chakoumakos, B. C.; Nagler, S. E. Low-Temperature Crystal and Magnetic Structure of α-RuCl3. *Phys. Rev. B* **2016**, *93* (13), 1−8.
(29) Banerjee, A.; Yan, J.; Knolle, J.; Bridges, C. A.; Stone, M. B.; Lumsden, M. D.; Mandrus, D. G.; Tennant, D. A.; Moessner, R.; Nagler, S. E. Neutron Scattering in the Proximate Quantum Spin Liquid α-RuCl3. *Science* **2017**, *356* (6342), 1055−1059.
(30) Banerjee, A.; Lampen-Kelley, P.; Knolle, J.; Balz, C.; Aczel, A. A.; Winn, B.; Liu, Y.; Pajerowski, D.; Yan, J.; Bridges, C. A.; et al. Excitations in the Field-Induced Quantum Spin Liquid State of α-RuCl3. *NPJ. Quantum Mater.* **2018**, *3* (1), 1−7.
(31) Yamada, M. G.; Fujita, H.; Oshikawa, M. Designing Kitaev Spin Liquids in Metal-Organic Frameworks. *Phys. Rev. Lett.* **2017**, *119* (5), 057202.
(32) Yoshida, H.; Michiue, Y.; Takayama-Muromachi, E.; Isobe, M. β-Vesignieite BaCu3V2O8(OH) 2: A Structurally Perfect S = 1/2 Kagomé Antiferromagnet. *J. Mater. Chem.* **2012**, *22* (36), 18793−18796.
(33) Zhang, B.; Zhang, Y.; Wang, Z.; Wang, D.; Baker, P. J.; Pratt, F. L.; Zhu, D. Candidate Quantum Spin Liquid Due to Dimensional Reduction of a Two-Dimensional Honeycomb Lattice. *Sci. Rep.* **2014**, *4* (1), 6451.
(34) Zhang, B.; Baker, P. J.; Zhang, Y.; Wang, D.; Wang, Z.; Su, S.; Zhu, D.; Pratt, F. L. Quantum Spin Liquid from a Three-Dimensional Copper-Oxalate Framework. *J. Am. Chem. Soc.* **2018**, *140* (1), 122−125.
(35) Kong, J. J.; Jiang, Y. X.; Zhang, J. C.; Shao, D.; Huang, X. C. Two-Dimensional Magnetic Materials of Cobalt(Ii) Triangular Lattices Constructed by a Mixed Benzimidazole-Dicarboxylate Strategy. *CrystEngcomm* **2019**, *21* (15), 2596−2604.
(36) Misumi, Y.; Yamaguchi, A.; Zhang, Z.; Matsushita, T.; Wada, N.; Tsuchiizu, M.; Awaga, K. Quantum Spin Liquid State in a Two-Dimensional Semiconductive Metal−organic Framework. *J. Am. Chem. Soc.* **2020**, *142* (39), 16513−16517.
(37) Sorolla, M.; Wang, X.; Koo, H. J.; Whangbo, M. H.; Jacobson, A. J. Synthesis of the Elusive S = 1/2 Star Structure: A Possible Quantum Spin Liquid Candidate. *J. Am. Chem. Soc.* **2020**, *142* (11), 5013−5016.
(38) Burzurí, E.; Martínez-Pérez, M. J.; Martí-Gastaldo, C.; Evangelisti, M.; MañMañAs-Valero, S.; Coronado, E.; Martínez, J. I.; Galan-Mascaros, J. R.; Luis, F. A Quantum Spin Liquid Candidate Isolated in a Two-Dimensional CoIIRhIII Bimetallic Oxalate Network. *Chem. Sci.* **2023**, *14* (14), 3899−3906.
(39) Liu, H.; Khaliullin, G. Pseudospin Exchange Interactions in D7 Cobalt Compounds: Possible Realization of the Kitaev Model. *Phys. Rev. B* **2018**, *97*, 1.
(40) Liu, L.; Li, L.; DeGayner, J. A.; Winegar, P. H.; Fang, Y.; Harris, T. D. Harnessing Structural Dynamics in a 2D Manganese−Benzoquinoid Framework To Dramatically Accelerate Metal Transport in Diffusion-Limited Metal Exchange Reactions. *J. Am. Chem. Soc.* **2018**, *140* (36), 11444−11453.
(41) Liu, L.; Degayner, J. A.; Sun, L.; Zee, D. Z.; Harris, T. D. Reversible Redox Switching of Magnetic Order and Electrical Conductivity in a 2D Manganese Benzoquinoid Framework. *Chem. Sci.* **2019**, *10* (17), 4652−4661.
(42) Jeon, I. R.; Negru, B.; Van Duyne, R. P.; Harris, T. D. A 2D Semiquinone Radical-Containing Microporous Magnet with Solvent-Induced Switching from Tc = 26 to 80 K. *J. Am. Chem. Soc.* **2015**, *137* (50), 15699−15702.
(43) DeGayner, J. A.; Jeon, I. R.; Sun, L.; Dincă, M.; Harris, T. D. 2D Conductive Iron-Quinoid Magnets Ordering up to Tc = 105 K via Heterogenous Redox Chemistry. *J. Am. Chem. Soc.* **2017**, *139* (11), 4175−4184.
(44) Sahadevan, S. A.; Abhervé, A.; Monni, N.; Sáenz De Pipaón, C.; Galán-Mascarós, J. R.; Waerenborgh, J. C.; Vieira, B. J. C.; Auban-Senzier, P.; Pillet, S.; Bendeif, E. E.; et al. Conducting Anilate-Based Mixed-Valence Fe(II)Fe(III) Coordination Polymer: Small-Polaron Hopping Model for Oxalate-Type Fe(II)Fe(III) 2D Networks. *J. Am. Chem. Soc.* **2018**, *140* (39), 12611−12621.
(45) Gao, B.; Chen, T.; Tam, D. W.; Huang, C. L.; Sasmal, K.; Adroja, D. T.; Ye, F.; Cao, H.; Sala, G.; Stone, M. B.; et al. Experimental Signatures of a Three-Dimensional Quantum Spin Liquid in Effective Spin-1/2 Ce2Zr2O7 Pyrochlore. *Nat. Phys.* **2019**, *15* (10), 1052−1057.
(46) Arh, T.; Sana, B.; Pregelj, M.; Khuntia, P.; Jagličić, Z.; Le, M. D.; Biswas, P. K.; Manuel, P.; Mangin-Thro, L.; Ozarowski, A.; et al. The Ising Triangular-Lattice Antiferromagnet Neodymium Heptatantalate as a Quantum Spin Liquid Candidate. *Nat. Mater.* **2022**, *21* (4), 416−422.
(47) Li, N.; Huang, Q.; Yue, X. Y.; Chu, W. J.; Chen, Q.; Choi, E. S.; Zhao, X.; Zhou, H. D.; Sun, X. F. Possible Itinerant Excitations and Quantum Spin State Transitions in the Effective Spin-1/2 Triangular-Lattice Antiferromagnet Na2BaCo(PO4)2. *Nat. Commun.* **2020**, *11* (1), 1−9.
(48) Bera, A. K.; Yusuf, S. M.; Kumar, A.; Ritter, C. Zigzag Antiferromagnetic Ground State with Anisotropic Correlation Lengths in the Quasi-Two-Dimensional Honeycomb Lattice Compound $Na_2Co_2TeO_6$. *Phys. Rev. B* **2017**, *95* (9), 094424.
(49) Samarakoon, A. M.; Chen, Q.; Zhou, H.; Garlea, V. O. Static and Dynamic Magnetic Properties of Honeycomb Lattice Antiferromagnets Na2M2TeO6, M = Co and Ni. *Phys. Rev. B* **2021**, *104* (18), 184415.
(50) Liu, H.; Chaloupka, J.; Khaliullin, G. Kitaev Spin Liquid in 3d Transition Metal Compounds. *Phys. Rev. Lett.* **2020**, *125* (4), 47201.
(51) Sahling, S.; Lorenzo, J. E.; Remenyi, G.; Marin, C.; Katkov, V. L.; Osipov, V. A. Heat Capacity Signature of Frustrated Trimerons in Magnetite. *Sci. Rep.* **2020**, *10* (1), 1−6.
(52) Zhong, R.; Guo, S.; Cava, R. J. Frustrated Magnetism in the Layered Triangular Lattice Materials K2Co(SeO3)2 and Rb2Co(SeO3)2. *Phys. Rev. Mater.* **2020**, *4* (8), 1−8.

https://doi.org/10.1021/jacs.3c14537
J. Am. Chem. Soc. 2024, 146, 15061−15069

(53) Koteswararao, B.; Kumar, R.; Khuntia, P.; Bhowal, S.; Panda, S. K.; Rahman, M. R.; Mahajan, A. V.; Dasgupta, I.; Baenitz, M.; Kim, K. H.; et al. Magnetic Properties and Heat Capacity of the Three-Dimensional Frustrated S= 12 Antiferromagnet PbCuTe2 O6. *Phys. Rev. B - Condens. Matter Mater. Phys.* **2014**, *90* (3), 1−7.
(54) Zhong, R.; Guo, S.; Xu, G.; Xu, Z.; Cava, R. J. Strong Quantum Fluctuations in a Quantum Spin Liquid Candidate with a Co-Based Triangular Lattice. *Proc. Natl. Acad. Sci. U. S. A.* **2019**, *116* (29), 14505−14510.
(55) Li, Y.; Liao, H.; Zhang, Z.; Li, S.; Jin, F.; Ling, L.; Zhang, L.; Zou, Y.; Pi, L.; Yang, Z.; et al. Gapless Quantum Spin Liquid Ground State in the Two-Dimensional Spin-1/2 Triangular Antiferromagnet YbMgGaO4. *Sci. Rep.* **2015**, *5* (1), 16419.
(56) Xing, J.; Sanjeewa, L. D.; Kim, J.; Stewart, G. R.; Podlesnyak, A.; Sefat, A. S. Field-Induced Magnetic Transition and Spin Fluctuations in the Quantum Spin-Liquid Candidate CsYbSe2. *Phys. Rev. B* **2019**, *100* (22), 1−8.

https://doi.org/10.1021/jacs.3c14537
J. Am. Chem. Soc. 2024, 146, 15061−15069